Journal of Hazardous Materials 494 (2025) 138678

Contents lists available at ScienceDirect

Journal of Hazardous Materials

journal homepage: www.elsevier.com/locate/jhazmat

Treatment of PFAS-laden solids via fluidized bed gliding arc plasmatron

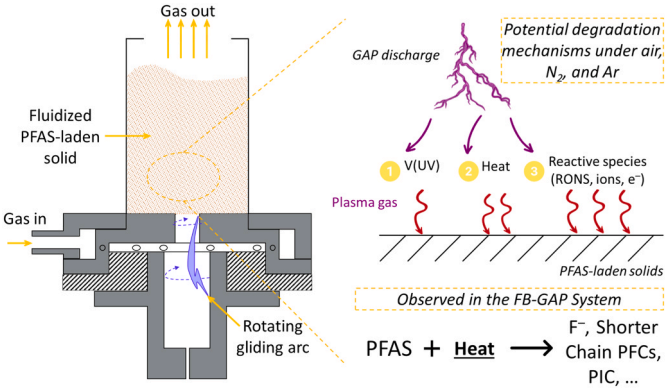
Jimmy Murillo-Gelvez [a,*], Alexander Rabinovich [b], Christopher M. Sales [c], Alexander Fridman [b], Gregory Fridman [d], Erica R. McKenzie [a]

[a] Civil and Environmental Engineering, Temple University, Philadelphia, PA, United States
[b] Drexel University C. & J. Nyheim Plasma Institute, Camden, NJ, United States
[c] Civil, Architectural, and Environmental Engineering, Drexel University, Philadelphia, PA, United States
[d] AAPlasma LLC, Philadelphia, PA, United States

HIGHLIGHTS

- A fluidized bed gliding arc plasmatron (FB-GAP) degraded PFAS-contaminated sand within 30 minutes.
- Higher plasma powers increased temperature, enhancing PFAS removal and confirming thermolysis as the main mechanism.
- Adding methane as auxiliary gas enabled plasma-assisted combustion and significantly lowered treatment costs.
- The fluorine mass balance, based on measurements from gas-phase base traps and treated solids, was ~20%.
- Recirculating effluent gas through the GAP is proposed to eliminate products of incomplete combustion (PIC).

GRAPHICAL ABSTRACT



ARTICLE INFO

Keywords:
Fluorinated
Surfactants
Degradation
Defluorination
Thermolysis

ABSTRACT

The extensive use and recalcitrance of per- and polyfluoroalkyl substances (PFAS) have caused soil and water contamination across the globe. Most PFAS destruction technologies are applied to aqueous matrices; there is a need for technologies that can effectively treat PFAS-contaminated solids. In this study, a fluidized bed gliding arc (non-thermal) plasma reactor (FB-GAP) was used to treat PFAS-laden sand under different gas discharges. Argon plasma did not degrade PFAS, suggesting there is no dissociative electron attachment in dry gas. Similar parent compound degradation and defluorination extents were observed under air- and nitrogen-discharges, implying that thermolysis was the main PFAS degradation process. The use of methane as an auxiliary gas increased maximum temperatures and reduced treatment costs through plasma-assisted combustion of a lean fuel mix. The fluorine mass balance was ~20 % after accounting for fluoride and targeted PFAS in treated solids and aqueous base traps for the effluent gas. The difference (~80 %) likely resulted from irreversible reactions with SiO_2 or formation of volatile organofluorine compounds. Further treatment of the effluent gas through the

* Correspondence to: Center for PFAS Solutions, New Castle, DE, United States.
E-mail address: jimmy.murillo.gelvez@pfasolutions.org (J. Murillo-Gelvez).

https://doi.org/10.1016/j.jhazmat.2025.138678
Received 29 January 2025; Received in revised form 14 April 2025; Accepted 18 May 2025
Available online 19 May 2025
0304-3894/© 2025 Elsevier B.V. All rights are reserved, including those for text and data mining, AI training, and similar technologies.

plasmatron is proposed as an alternative to fully mineralize PFAS. The results from this study demonstrate that non-equilibrium plasma technologies are a promising treatment option for PFAS-laden solids.

1. Introduction

Per- and polyfluoroalkyl substances (PFAS) have been widely used in multiple industries [1–5] due to their unique physicochemical properties conferred by the recalcitrant C-F bonds and, for some PFAS, the hydrophilicity of the acidic (carboxylic, sulfonic) headgroups. The same properties that make these substances useful (e.g., chemical inertness, water/oil repellency) are responsible for the observed bioaccumulation (of some PFAS) [6–10] and pervasive contamination of soil [11,12], groundwater [13,14], and surface water [15–17] worldwide. Given the recalcitrance, bioaccumulative potential, and toxicity of PFAS, it is imperative to develop cost-effective technologies that remove and mineralize these contaminants.

Most PFAS destruction technologies developed to date are applied to aqueous matrices, including non-thermal plasma [18–20], supercritical water oxidation (SCWO) [21,22], hydrothermal alkaline treatment (HALT) [23,24], electrochemical oxidation [25,26], and UV-generated hydrated electrons [27,28]. There are only a few alternatives for the direct treatment of dry PFAS-laden solids, including thermal desorption or destruction (e.g., incineration, smoldering, reactivation) [29–33] and ball milling [34,35]. Informed by the more mature aqueous PFAS treatment methodologies, many solids treatment approaches rely on the desorption of PFAS from contaminated solids (e.g., through soil washing [36,37] or foam fractionation [38]) followed by treatment of the PFAS-laden solution. Despite the relatively good mass removals, these approaches remain, in many instances, time intensive and/or cost prohibitive [39]. Therefore, there is a need for technologies that can cost-effectively treat PFAS-contaminated solids.

Dry thermal processes such as smoldering and combustion have been proven to remove parent PFAS from solid matrices. PFAS mass removals typically exceed 99 % within a few hours of treatment, but high temperatures are needed (>1000°C) to minimize gaseous perfluorocarbon emissions (i.e., achieve complete mineralization) [31,40]. The high operational costs and the generation of products of incomplete combustion (PIC) represent critical barriers in the widespread adoption and deployment of thermal-based technologies [41–44].

A promising alternative to treat PFAS-laden solids is the use of non-equilibrium plasma, which has been shown to be effective at degrading PFAS in aqueous matrices [45–47]. In non-equilibrium plasma discharges, electrons in the feed gas are excited and their temperature is much higher than that of the rest of the gas (i.e., "non-equilibrium") [48]. Irrespective of the type of discharge (e.g., dielectric barrier discharge (DBD) or gliding arc plasmatron (GAP)), non-equilibrium plasmas create a reactive environment that may degrade PFAS through a combination of heat, ultraviolet and visible (UV-Vis) radiation, and reaction with free electrons and reactive species (e.g., reactive oxygen and nitrogen species, RONS) [49]. This highly reactive environment is tunable by controlling the power and the feed gas type, making non-equilibrium plasma an attractive candidate for the efficient degradation of recalcitrant contaminants such as PFAS. To date, only one study has evaluated the applicability of non-thermal plasma to directly treat dry PFAS-laden solids [50]. Although significant PFAS mass removals were observed by Zhan et al. (>70 %), the degradation mechanism was unclear, and the scalability of the process was limited. More work is needed to better understand the factors that control the degradation of PFAS in non-thermal plasma treatments and further develop this technology for scale-up.

In this study, a GAP reactor was used to generate plasma discharges and treat PFAS-laden sand in a fluidized bed configuration—a scalable treatment process. The effect of feed gas (air, nitrogen, and argon), auxiliary gas (methane), and temperature (heat released from the plasma discharge) on PFAS removal is discussed. The potential mechanism(s) and measured degradation products are presented. The results from this study demonstrate that non-equilibrium plasma technologies are a promising alternative for the treatment of PFAS-laden solids.

2. Materials and methods

2.1. Chemicals

Perfluorobutanoic acid (PFBA), perfluorooctanoic acid (PFOA), potassium perfluorobutanesulfonate (PFBS), potassium perfluorohexanesulfonate (PFHxS), potassium perfluorooctanesulfonate (PFOS), acetic acid (Glacial, Reagent Plus, ≥99 %), ammonium acetate (≥99 %), ammonium chloride, disodium ethylenediaminetetraacetate dihydrate (EDTA), LC/MS grade methanol (OmniSolv®), and aluminum phthalocyanine chloride (AlPc-Cl) were purchased from Sigma-Aldrich (Allentown, PA, USA). Sodium 1H,1H,2H,2H-perfluorooctanesulfonate (6:2 fluorotelomer sulfonate, 6:2FTS) was obtained from Toronto Research Chemicals. A standard mix of 24 native PFAS (PFAC-24PAR) and a mix of 19 mass-labeled PFAS (MPFAC-24ES; extraction standard [ES]) were obtained from Wellington Laboratories (Guelph, ON, Canada). Ammonium hydroxide, optima LC/MS grade water, sodium fluoride (NaF, >99 %), and reagent alcohol (HPLC grade) were purchased from ThermoFisher Scientific (Fairlawn, NJ, USA).

2.2. Sample preparation

All PFAS-laden solids in this study consisted of laboratory spiked sand. All-purpose sand (Quikrete®) was dry sieved to obtain a relatively homogeneous particle size (0.450 mm - 1 mm). Sieved solids and methanol were mixed at a ratio of 1 mL of methanol per 1 g of sand in a high-density polyethylene (HDPE) bottle and spiked with a mix of PFBA, PFOA, PFBS, PFHxS, PFOS, and 6:2FTS, each at a nominal concentration of 3–4 μg/g — as different batches were prepared throughout the study, the concentrations of each of the six PFAS were measured before each test (concentrations at time zero). Thorough mixing of the slurry was performed for 15 min in an orbital shaker at 280 RPM. The bottle was then placed in a fume hood for at least 3 days to remove the methanol through evaporation. Complete evaporation was ensured by mixing the contents periodically and confirmed visually.

2.3. Gliding arc plasmatron (GAP) and degradation experiments

A fluidized bed GAP reactor (FB-GAP) was built by adapting a stainless-steel pipe (reactor body; length: 35.5 cm; diameter: 3.6 cm), in which the contaminated solids were loaded and treated, to the outlet of a plasmatron (Fig. S1); the upward gas flow ensured the fluidization of the solids. Gas (air, nitrogen, or argon) was fed at variable flow rates (typically 40 L/min) tangentially to the cylindrical plasmatron body, creating a gas vortex that was ionized due to the electrodes' voltage difference. The plasma arc rotated and stretched, gliding on the high voltage and ground electrodes, as a function of gas flow rate, current, and breakdown voltage of the gas. The flow rate (40 L/min) was chosen through preliminary experiments to ensure plasma discharge stability and minimize solid losses in the open (i.e., unsealed) FB-GAP system. Flow rates > 40 L/min generally decreased plasma jet temperature and increased solid losses while flow rates < 40 L/min did not provide the vortex necessary for the gliding arc to exist. The column of solids inside the reactor body (typically 650 g) was physically separated from the plasmatron by a 450 μm stainless-steel grounded mesh; therefore, only reactive species and heat released from the plasmatron were expected to

interact with the contaminated solids. While previous studies indicate that grounded meshes can neutralize reactive species [51], the thin mesh used in this study was not anticipated to interfere. The temperature within the reactor was tracked using a stainless-steel thermocouple probe which was located 5 cm above the plasmatron (Fig. S1). Although a vertical temperature gradient may have developed inside the reactor, no other temperature measurements were collected; it was assumed that the temperature was relatively homogeneous due to the fluidization of the treated solids.

To avoid clogging the plasmatron, solids were loaded while air was flowing through the reactor. The initial and final reaction times were operationally defined and corresponded to the times when the power source (to generate the plasma discharge) was turned on and off, respectively. In the unsealed FB-GAP reactor (Fig. S1), solid samples were collected from the center of the column with a long handheld stainless-steel spoon every 10 minutes. The total treatment duration extended up to 60 minutes. Negligible losses of solid material (< 2 %) were observed during these experiments. All solid samples were extracted and analyzed in triplicates. In selected runs (denoted as plasma assisted combustion experiments), methane was fed as the auxiliary gas (at variable flow rates 1 – 3 L/min) and experiments were run as previously described.

As an attempt to measure semi-volatile PFAS and hydrofluoric acid (HF) or fluoride, the FB-GAP was sealed (Fig. S2), and the off gas passed through four base traps (500 mL of 0.1 M NaOH) in series. Only the initial and final solid samples were collected, which were extracted and analyzed as described below (Section 2.5). An aliquot of the base trap solutions (0.5 mL) was mixed with an equal volume of 1 % acetic acid in methanol, spiked with 1 ng ES, and centrifuged at 13000 RPM for 30 min to remove fine particles. The clean supernatant (0.7 mL) was transferred to a new 2 mL polypropylene (PP) centrifuge vial and used for PFAS analysis. Fluoride measurements were directly performed with the base trap solutions after adding total ionic strength adjustment buffer III (TISAB III) as described in Section 2.6. Calibration curves and spike-recovery tests with and without NaOH added confirmed a negligible effect of pH on the spectrophotometric response (data not shown).

2.4. Furnace tests

A Fisher isotemp 650/750 series programmable muffle furnace was used to conduct experiments in which thermolysis was expected to be the only degradative process. Solids (3.5 g) were loaded into ceramic crucibles – without lid – and left to react at variable temperatures for determined periods. The temperature was either varied during the run, if a temperature profile observed in GAP experiments was being matched, or fixed, if only a set temperature was being evaluated.

2.5. PFAS extraction and analysis

PFAS were extracted from solids using a modified version of the procedure described by Nickerson et al. [52] for anionic PFAS. Briefly, 1 g of sample was spiked with 2 ng of ES and mixed with 8 mL of 1 % (v/v) ammonium hydroxide in methanol in a 50 mL PP vial. The resulting slurry was vortexed for 30 seconds, sonicated at 30°C for 15 minutes, and centrifuged for 20 minutes at 3000 RPM. The supernatant was collected in a new 50 mL PP centrifuge vial. The extraction procedure was repeated three more times, and the supernatants were pooled in the same 50 mL centrifuge vial. The pooled extract was evaporated to dryness in a water bath (60°C) under a gentle stream of nitrogen. The resulting dry sample was reconstituted in 1 mL of 1 % acetic acid in methanol. The reconstituted solution was vortexed for 10 seconds, and half of the volume of the clean sample (0.5 mL) was transferred to a new 2 mL centrifuge vial containing 0.5 mL of LC/MS grade water. Aliquots (50 µL) were transferred for PFAS analysis, and the rest archived at 4°C. Extracts exceeding the PFAS quantitation range (e.g., for spiked, untreated samples) were further diluted with a water-methanol (50:50) solution containing ES at 1 µg/L prior to analysis.

Separation and detection of PFAS analytes was achieved using an Exion LC coupled with a X500R QTOF mass spectrometer (Sciex, USA; LC-QToF-MS). A Gemini C-18 column (50 × 3 mm, 3 µm; Phenomenex, USA) and guard column were used and maintained at 40 °C. A delay column (Luna C-18, 30 × 5 mm, 5 µm; Phenomenex, USA) was installed to minimize PFAS background contamination in the quantification windows. The analytes were eluted using 10 mM ammonium acetate in LC/MS grade water (Solvent A) and 10 mM ammonium acetate in LC/MS grade methanol (Solvent B) at a flow rate of 500 µL/min with the following gradient (A%/B%): 99/1 (0 min), 99/1 (0.25 min), 50/50 (0.50 min), 1/99 (4.50 min), 1/99 (8.50 min), 99/1 (10 min), 99/1 (13 min). The total run time was 13 minutes, and the injection volume was 10 µL. The mass spectrometer was operated in negative electrospray ionization (ESI−). Mass-labeled extraction standards were utilized to quantify PFAS analytes (i.e., isotope dilution) with scheduled high resolution multiple reaction monitoring. The electrospray ionization capillary voltage was −4.5 kV with source temperature of 500 °C. The mass transitions, declustering potentials, and collision energies can be found elsewhere [53]. PFAS analytes and paired ES, their typical recoveries, and quality assurance and control elements can be found in the supplementary information (Section S2, Table S1).

2.6. Fluoride extraction and analysis

Fluoride was extracted from (un)treated solids by mixing 1 g of sand with 3 mL of 10 mM sodium hydroxide (in water) in a 15 mL PP vial [54]. The slurry was vortexed for 30 seconds, sonicated at 30°C for 15 minutes, and centrifuged at 4000 RPM for 20 minutes. The supernatant was collected in a new 15 mL PP vial, and the extraction procedure was repeated once more. A portion (1.8 mL) of the resulting pooled extract was mixed with 0.2 mL of TISAB III (made in house – Supplementary information Section S3) in a 2 mL PP centrifuge vial. TISAB III was needed to achieve nearly-complete fluoride recoveries in spike-recovery experiments (Fig. S3). The contents were vortexed for 10 seconds and then centrifuged at 13000 RPM for 30 min to remove fine particles. The clean supernatant (1 mL) was transferred to a new 2 mL PP centrifuge vial and used for fluoride analysis. Spiked controls (with sodium fluoride) were included in each batch; results were considered valid if recoveries were within 80–120 % of the expected values. Selected extracts and aqueous samples with fluoride concentrations at or below the level of quantification (LOQ, typically ~10 µM) were concentrated through evaporation and re-analyzed.

Fluoride was measured following the spectrophotometric method by Chatterjee et al. [55] with a few modifications. To a 2 mL PP centrifuge vial containing 1850 µL of reagent alcohol (~90 % ethanol), 50 µL of the sensor (135 µM AlPc-Cl in reagent alcohol) and 50 µL of the prepared samples (solid extracts or aqueous samples with TISAB III) were added. The contents were vortexed for 5 seconds, poured into 1 cm quartz cuvettes, and the absorbance was measured in an Agilent 8453 UV–visible spectroscopy system. As shown in Chatterjee et al.'s work, the absorbance at ~672 nm decreases with increasing concentration of fluoride (Fig. S4).

2.7. Data analysis

2.7.1. Kinetics of mass removal – first order rates

In selected cases, the kinetics of parent PFAS degradation/removal were analyzed via a first order model (Eq. 1)

$$\ln\frac{C_t}{C_0} = -k_{Obs} * t \quad (1)$$

where C_t is the concentration of PFAS at a given time t, C_0 is the initial PFAS concentration at time zero, and k_{Obs} is the observed first order rate constant.

2.7.2. Specific energy input (SEI)

To compare the energy efficiency of different treatment conditions, the specific energy input (i.e., the energy used per mass of contaminated solid) was calculated using Eq. 2. The time used for the calculation was the point at which a mass removal ≥ 90 % (i.e., ≥ one order of magnitude) was attained for a selected parent PFAS. Note that this equation is analogous to the electrical energy per order of magnitude (EE/O) calculation typically used for aqueous systems [28,56].

$$SEI(kJ/g) = \frac{Power(kW) * time(s)}{treated\ mass(g)} \quad (2)$$

2.7.3. Defluorination extent

The fluoride measured in the aqueous extracts ($[Fluoride]_S$) and the base traps ($[Fluoride]_{BT}$) was compared to the total fluorine expected from the parent PFAS to determine the extent of defluorination (Eq. 3)

$$Defluorination(\%) = \frac{[Fluoride]_S * mass\ treated + \sum([Fluoride]_{BT} * V_{BT})}{\sum([PFAS]_0 * mass\ treated * \#Fluorine\ atoms)} * 100 \quad (3)$$

where $[PFAS]_0$ is the initial concentration of a given PFAS compound on the contaminated solid (μmol/g sand) and V_{BT} is the volume in the base traps.

3. Results and discussion

A discussion of PFAS mass removals and associated mechanisms is presented in Sections 3.1 and 3.2. Information on measured degradation products and the implications on PFAS fate and transport is presented in Section 3.3. Table S2 in the supporting information lists all the conditions tested and measurements performed on the (un)treated materials.

3.1. Parent PFAS mass removals and mechanism

The FB-GAP reactor achieved nearly complete mass removals of the parent PFAS — PFBA, PFOA, 6:2FTS, PFBS, PFHxS, and PFOS — after an hour of treatment at a fixed power of 630 W under air (Fig. 1). Around 5 % of the perfluoroalkyl sulfonic acids (PFSA) remained on the sand, suggesting that PFSA are more recalcitrant than perfluoroalkyl carboxylic acids (PFCA). The fluorotelomer sulfonate, however, exhibited a similar degradation profile as that of PFCAs (Fig. 1), suggesting that the presence of CH_2 units in the chain renders the molecule more amenable to degradation. Given the similarities in the degradation profiles of short and long chain PFAS (e.g., PFBS and PFOS), it can be concluded that the main mass removal processes are not chain-length dependent.

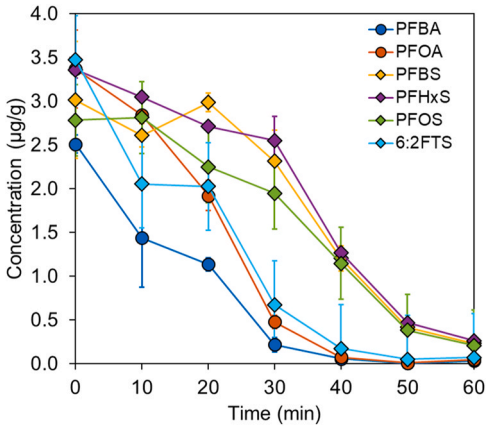


Fig. 1. Kinetics of PFAS degradation in the fluidized GAP reactor (FB-GAP). Conditions: 40 L air/min, 630 W, and 650 g of sand. Data represent the average concentration ± one standard deviation of triplicate samples (i.e., three replicates [from a single experiment] processed separately).

Since the degradation/defluorination of PFAS in water via non-equilibrium plasma is more energy efficient under argon than under air [57–59], argon was tested as the feed gas in the fluidized bed reactor. No PFAS transformation occurred within 60 minutes of solids treatment (Fig. 2). In aqueous system, dissociative electron attachment-electron transfer is believed to be the main PFAS degradation mechanism under argon discharges [57], therefore the full recovery of parent compounds from the solids suggests that this degradation mechanism does not readily occur in a dry gaseous environment. Besides the potential contribution of reactive species, the temperature developed with argon marginally surpassed that in the test with air at 480 W (Fig. 2); the low breakdown voltage of argon [60] impeded attaining higher powers and consequently, higher temperatures.

As illustrated with PFOS, decreasing the power input from 630 W to 480 W resulted in no mass removal (Fig. 2). This was likely a result of the low temperatures developed at 480 W—while at 630 W the system reaches ~400 °C within 60 minutes, the temperature does not surpass 150 °C in the same period at 480 W (Fig. 2B). Mass removals for all six parent PFAS for all conditions tested are presented in Fig. S5. Congruently, increasing the power of the plasma source led to higher temperatures, which in turn accelerated the PFAS mass removals (comparison of orange, blue, and purple data sets [Fig. 2]) and made more obvious the recalcitrance of PFSA (Fig. S5C). Although the final temperature developed under nitrogen at 780 W was similar to the temperature attained under air at 660 W, relatively higher temperatures were attained in a shorter period (350°C within 10 minutes). This resulted in faster PFOS removal, with > 99 % of the PFAS mass removed within 30 minutes. Under moisture-free nitrogen, *little to no RONS are expected* [61,62]; therefore, the observed mass removals can be fully ascribed to thermal processes (i.e., thermolysis and/or thermal desorption). Information on measured degradation products is presented in Section 3.3.

Plasma discharges may degrade PFAS through UV radiation, heat, and/or via reaction with RONS; however, the conclusions derived from the data shown in Fig. 2 suggest that thermal processes alone may be responsible for the observed parent compound removals. To test whether heat was the main PFAS removal process, the temperature profile observed in the FB-GAP reactor under air at 630 W (Figs. 1 and 2) was reproduced in a muffle furnace and spiked sand was directly treated in ceramic crucibles (samples were collected at different time points [Fig. 3]). The similarity in the PFAS concentration profiles indicates that thermolysis (i.e., degradation due to heat) was the *main* process responsible for the observed mass removals. PFCA and 6:2FTS exhibited appreciable mass removals at temperatures > 130 °C, while PFSA required temperatures > 350 °C. The higher recalcitrance of PFSA, the chain length independent degradation, and the onset mass removal temperatures are consistent with previous observations in thermal degradation studies [63–65], further supporting that thermolysis was the main driver for PFAS mass removals in the FB-GAP reactor.

Although the temperature was variable in each of the runs, constantly increasing as a function of time (Fig. 2B), the kinetics of PFAS mass removals were relatively constant after a specific onset (Fig. S6). In the experiment with air at 630 W, up to 50 % PFBA was removed at 20 minutes (Fig. 1); however, only thereafter did the removal occurred at a seemingly constant observed first-order rate constant (k_{Obs}), which is derived from the slope of the semilogarithmic plots (Eq. 1, Fig. S6). Only the data with a constant slope was considered for this analysis as discussed below and presented in Fig. S6.

Both carboxylic acids exhibited a similar k_{Obs} (0.16–0.17 min^{-1}), which was ~30 % higher than the rate constant observed for 6:2FTS. It is interesting that the apparent k_{Obs} were constant for most of the run regardless of the temperature increase from 270 °C at 20 min to 395 °C at 50 min. The k_{Obs} after the onset at 30 minutes (at ~350 °C) were the same for all three PFSA (0.08 min^{-1}), approximately half of the PFCA values (Fig. S6A-B). As previously discussed for Fig. 2, the kinetics were faster for the run with nitrogen; the k_{Obs} were approximately 2.5-fold

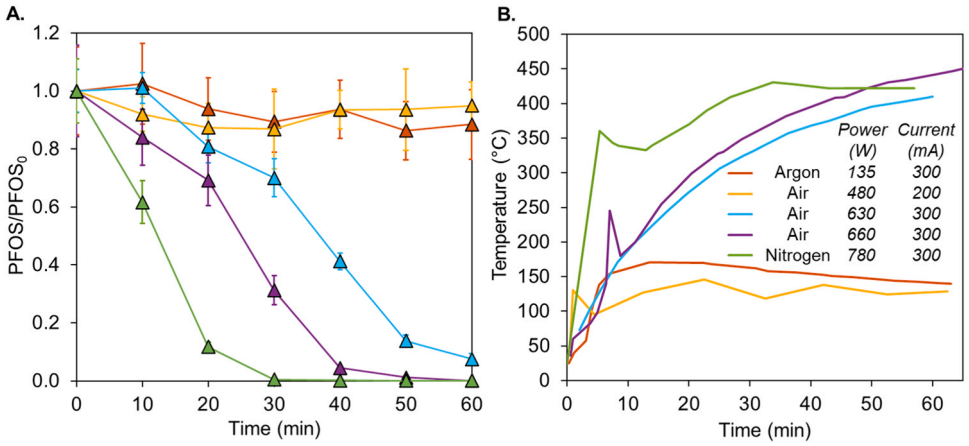


Fig. 2. The effect of gas type and power setting on A. PFOS mass removals and B. temperature profiles. The current was manually set, and the resulting power (listed in panel B.) was a function of the breakdown voltage of the gas. In all cases, 650 g of spiked sand were treated, and the gas flow rate was 40 L/min. Data represent the average concentration ± one standard deviation of triplicate samples.

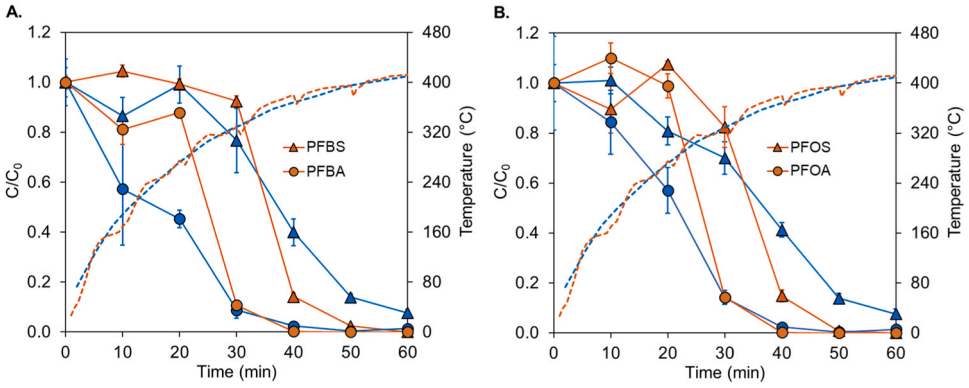


Fig. 3. Mass removals of A. PFBA and PFBS and B. PFOA and PFOS in the FB-GAP system (blue) and in a furnace (orange). The temperature profile (secondary y-axis) set in the furnace matched that developed in the FB-GAP system under air at 630 W (– – – for FB-GAP and – – – for furnace).

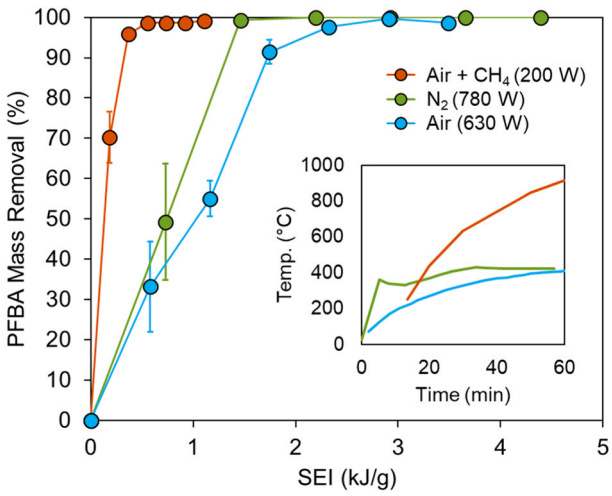
faster for the PFCA, PFSA, and the FTS when compared to the air treatment (Fig. S6). Under nitrogen, the onset for PFAS mass removals was 10 minutes (350 °C), and the temperature variations were lower than in the air run (350–420 °C), hence explaining the relatively constant mass removals. The relative reactivity among the PFAS classes investigated was also consistent in the N_2 run (i.e., the fluorotelomer sulfonate and the sulfonic acids were ~30 % and ~50 % less labile than the PFCA), demonstrating that the observed rates are likely driven by the same mass removal process (thermal desorption and/or thermolysis). The seemingly invariable, low concentrations – towards the end of the reaction – in Figs. S6C and S6D reflect mass removals > 99.98 % and 99.9 %, respectively. At such degradation extents (and low PFAS concentrations) further removal may be limited or cross-contamination may occur.

Despite any artifacts potentially introduced by the variable temperatures, our PFOA k_{Obs} matched the first order rate constants previously reported in a thermal degradation study (0.15 min^{-1} at 250°C and 0.3–0.4 min^{-1} at 300–400°C) [66], further indicating that thermal processes were likely responsible for the observed PFAS mass removals in the FB-GAP reactor. However, our PFOS degradation rates were ~10 times higher than those reported by the same authors at a slightly higher temperature of 450°C (0.2 vs 0.02 min^{-1}). In a more recent study, the same group reported k_{Obs} for PFSA thermal degradation in soils of 0.01–0.02 min^{-1} at 400 °C and 0.22–0.29 min^{-1} at 500 °C [67]. Since the degradation of PFOA exhibited similar kinetics irrespective of the matrix being treated (technical salt alone or in the presence of GAC [66], soil [67], or sand [this study]), the causes for the discrepancies in PFOS k_{Obs} are unclear and warrant further investigation.

3.2. Plasma assisted combustion

Given the critical role of temperature in the removal of PFAS, methane was fed as an auxiliary gas to attain higher temperatures through combustion. An important advantage of using plasma for the combustion process is that lean fuel mixtures can be used (i.e., plasma-assisted combustion) [68]. This allows attaining higher temperatures faster and at lower energy inputs, potentially lowering treatment costs. Although different methane flow rates were tested (all ≤ 3 L CH_4/min with 40 L air/min), only one representative case is discussed below. In general, methane flow rates ≤ 1 L/min resulted in no appreciable combustion and > 2 but ≤ 3 L/min exhibited faster heating and increased final temperatures.

Although the PFAS removal rates were slower when methane was used as an auxiliary gas (e.g., compared to the nitrogen run; Figs. S7 and S5d), the SEI (electrical energy used to treat a given mass of contaminated solid, Eq. 2) was significantly lower. The SEI required to remove > 95 % of PFBA in the FB-GAP with 2 L/min of methane (0.36 kJ/g) was *ca.* 4 times lower than the observed in the N_2 run at 780 W (1.40 kJ/g), whose SEI was in turn 1.5 lower than that in the treatment under air at 630 W (2.08 kJ/g, Fig. 4). The improved SEI stems from the higher temperatures attained with the addition of methane, reaching up to ~900 °C within one hour of treatment – twice as high as the generated with power inputs 3–4 times greater (inset Fig. 4). The lower SEIs, achieved with methane as an auxiliary gas, translate to treatment cost



Condition	Cost ($USD per 1,000 kg sand)
Air + CH_4 (200 W)	$46
N_2 (780 W)	$62
Air (630 W)	$93

Fig. 4. Comparison of specific energy inputs (SEI) for the removal of PFBA under air + methane, air, and nitrogen. The inset shows the temperatures developed in each case as a function of time. In all cases the air/N_2 flow rate was 40 L/min , 650 g of spiked sand were treated, and when applicable the methane flow rate was 2 L/min. Data represent the average ± one standard deviation of triplicate samples. The table lists the costs to achieve > 95 % PFBA mass removals per metric ton of sand treated (see calculations in Section S4.2.).

savings of ~ 26 % after considering the electricity and methane used (see Table in Fig. 4 and Section S4.2.). Note that the costs are even lower when compared to the air 630 W run (50 % savings) and could be further reduced through optimization, highlighting the scalability and economic viability of this treatment approach. The apparent dependency of the SEIs and PFAS mass removals on temperature suggests that PFAS degradation is also driven by heat (i.e., thermolysis) in the plasma-assisted combustion system.

As discussed in the introduction, to the best of our knowledge, Zhan et al.'s work (pulsed corona discharge plasma to treat PFOA-laden soil (300 mg/kg = 300 μg/g) [50]) is the only peer-reviewed publication to date on the use of non-equilibrium plasma for the direct treatment of PFAS-laden solids. In their system, a set power between 38 W and 62 W achieved similar PFOA mass removals; therefore, the 38 W condition will be used hereafter for comparison purposes. Under these settings, the authors achieved up to 71 % PFOA mass removal within 120 minutes, yielding an SEI of 54.7 kJ/g (5 g of soil were treated). Since the PFOA loading (on the contaminated solid) in Zhan et al.'s work was 70–80 times greater than the used in this study, a mass removal of 3 μg/g will be used as an arbitrarily defined limit (> 90 % mass removal in our work) to compare the SEI in both studies. For the air, N_2, and air + CH_4 runs, the SEI at 3 μg/g of PFOA removed were 1.90, 0.81, and 0.18 kJ/g, respectively (Fig. S8), all lower than the SEI in Zhan et al.'s work (2.23 kJ/g at the same mass removal extent). These numbers highlight the highly energy-efficient nature of the FB-GAP reactor, especially when methane is used as an auxiliary gas. Note that the SEI are normalized by the amount of treated material in a given period of time, which produces significantly lower specific energy inputs for the FB-GAP. This is unlikely to change the conclusion on the superiority of the FB-GAP system as the corona discharge system is harder to scale up. It is noteworthy that this comparison is not completely fair; e.g., the solid matrix in Zhan et al.'s work is more complex (soil rather than sand) and many of the soil constituents (e.g., OM, salts) may scavenge reactive species, reducing the effectiveness of the treatment. However, this provides a framework for comparison and illustrates the scalability and promising performance (from an energy-efficiency standpoint) of the FB-GAP system, particularly when methane is used as an auxiliary gas.

3.3. Degradation products

While thermal desorption may be a potential PFAS mass removal process in the FB-GAP system [29,30], the detection of shorter chain PFAS suggest that parent compound degradation may be occurring (Fig. S9a). Note that the PFAS solutions used to prepare the contaminated solids were made with technical salts and acids that may contain shorter chain perfluoroalkyl acids as impurities (e.g., PFBA, PFPeA, PFHxA, and PFHpA in PFOA [69] and PFHpS (up to 8 %) in PFOS-K [70]). Unfortunately, the concentration of these shorter chain acids was not determined for the untreated solids because dilutions were made prior to analysis to quantify the parent PFAS only. Thus, the potential contribution from impurities in the technical salts/acids to the presence of these compounds at later points in the treatment cannot be ruled out.

Although thermal degradation is non-specific (i.e., different bonds in a molecule are randomly broken), the potential formation of shorter chain perfluoroalkyl acids support the hypothesis that the first step in the thermal destruction of PFSA and PFCA is the scission of the bond between the alpha carbon and the headgroup (i.e., desulfonation or decarboxylation) [63]. However, the shorter chain PFAS accounted for < 1.5 % mol/mol of the parent PFAS. The measured short chain PFAS were even lower for the nitrogen run, likely because of the faster mass removals, representing < 0.2 % of the sum of the parent compounds on a per mole basis (Fig. S9b). Since the measured perfluoroalkyl acids only accounted for a small fraction of the PFAS degraded, the remaining products were likely 1) more volatile and escaped the system through the effluent gas (off-gas hereafter), 2) not amenable to the analytical methods/tools used (e.g., trifluoroacetic acid [TFA]), and/or 3) further mineralized (i.e., fluoride formation).

The fluoride extracted from the treated solids increased as a function of time and accounted for up to ~15 % and ~20 % of the total fluorine initially present in the sand (calculated from the parent PFAS in the untreated sand, Eq. 3) in the air (630 and 660 W) and nitrogen (780 W) runs, respectively (Fig. 5). These results are consistent with previous thermal degradation studies reporting similar maximum defluorination extents (15–25 %) at ~400°C [66,67], which may be explained by the three reasons stated above and/or potential reactions between fluorine radicals and the steel reactor [71] or the silicates in the treated solids [67]. The higher temperatures and faster PFAS degradation observed under N_2 were likely the main drivers for the slightly larger defluorination. The measurable defluorination further demonstrates that the observed PFAS mass removals were caused, in part, by mineralization of the parent PFAS, not simply by thermal desorption. There is a small difference between the fluoride yields in the air FB-GAP experiment at 630 W and the furnace test (Fig. 5), with nearly identical results after 60 minutes of reaction. The initial difference might have been caused by

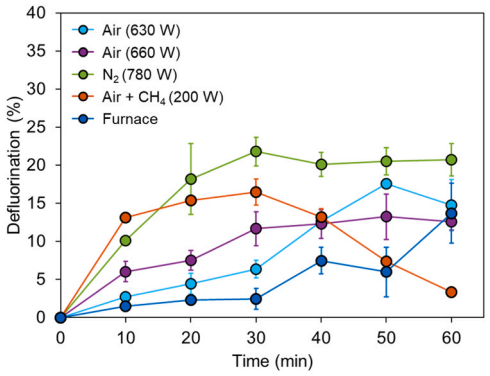


Fig. 5. Defluorination extents observed in four different FB-GAP runs (using air + methane, air, and nitrogen) and in the furnace experiments presented in Fig. 3. The base gas (air or nitrogen) was fed at 40 L/min and the methane flow rate was 2 L/min. The defluorination was calculated based on the fluoride extracted from the solids and the total fluorine expected from the initial concentration of the six parent PFAS. Data represent the average ± one standard deviation of triplicate samples.

more efficient heating in the FB-GAP system. However, the similarity in defluorination extents and PFAS mass removals (Fig. 2) further supports thermolysis as the primary PFAS degradation mechanism in the FB-GAP reactor, with a potentially minor contribution from RONS. Given the important role of reactive species in PFAS degradation in plasma-based technologies for the treatment of aqueous matrices [72–74], future studies should investigate the formation, fate, and reactivity of RONS in systems treating solids.

The defluorination extent reaches a similar maximum of ~17 % when methane is used as an auxiliary gas (Fig. 5), but it decreases to < 5 % at temperatures > 450°C. Since no apparent decrement in fluoride was observed for runs with no fuel added (see Air 660 W and Nitrogen 780 W, Fig. 5), the higher temperatures reached through methane combustion likely decrease the fluoride yields through 1) HF losses (i.e., volatilization) and/or 2) reaction of fluorine with silicon—sand is mostly SiO_2—leading to fluorine losses to the gas phase (e.g., as silicon tetrafluoride, SiF_4) or through irreversible binding to the solids. If HF is formed, it is expected to be recovered in the base traps (discussed below in Section 3.3.1.). Potential side reactions of fluorine, on the other hand, could lead to compounds that are beyond the analytical methods employed in this study, creating a gap in the mass balances. Consistent with our observations, Alinezhad et al. found that the fluoride yields from PFOA thermal degradation peaked at 400°C (25 %) but decreased at higher temperatures, yielding ~12 % defluorination at 500°C. Additionally, the same authors found that the presence of an aluminosilicate (kaolinite) drastically decreases the fluoride yields, likely as a consequence of chemisorption of F radicals on the mineral [67].

To test the effect of the treatment temperature on the recovery of fluoride, sand spiked with sodium fluoride was added to porcelain crucibles, dried at 105°C, and subsequently treated at 450°C and 800°C for 30 minutes in a muffle furnace (Fig. S10). As observed in the experiments with PFAS, the amount of fluoride recovered from NaF-spiked sand decreased as the temperature increased. Note that even at 450° the fluoride recovery was ~50 %. El-Attar et al. showed that direct ignition of NaF in the absence and presence of SiO_2 could lead to 7 % and 100 % fluorine losses, respectively [75]. Therefore, our observations and those of El-Attar et al. suggest that the most likely cause for the observed fluorine losses in the FB-GAP is the reaction with silicon in sand. Since a major product of the reaction between quartz (SiO_2) and fluorine is SiF_4 [76] and its hydrolysis may not yield 100 % F^- [77,78], the fluoride recovery in aqueous traps that receive the off-gas may not be complete.

3.3.1. *Products in the effluent gas of the FB-GAP reactor*

The reactor was modified to allow for sampling of the effluent gas as most of the PFAS mineralization products are likely volatilized at the temperatures reached in the FB-GAP, especially when methane is used as an auxiliary gas. The top part of the reactor was sealed, and the gaseous stream was passed through four 500 mL base traps (0.1 M NaOH) connected in series, all immersed in an ice bath (Fig. S2). In this configuration, the FB-GAP was operated with and without methane to understand the effect of higher temperature on the product distribution. In both cases, the PFAS mass removals from the solids were greater than 99 %, thus, only the transformation products/defluorination extents are discussed below.

The first base trap collected fine particles as qualitatively evidenced through a brown-reddish coloration (not shown). Although sand was sieved to > 0.450 mm, fine particles may have been associated with bigger grains (no wet sieving or washing of the sand was conducted). Moreover, the combined effect of fluidization (mechanical motion) and high temperatures may have eroded some of the particles and created finer grains. In addition to the accumulation of solids, *ca.* 35 mL of water were retrieved in the first trap in the treatment with methane as an auxiliary gas. This excess water likely resulted from the combustion of methane, which then condensed in the trap. The presence of water vapor throughout the reaction may contribute to the mineralization of PFAS, for instance, through the hydrolysis of perfluorinated acyl fluorides (RCOF), proposed to be a main thermal degradation product of PFAS [76,79–81].

The six PFAS initially present in the contaminated sand—and to a lower extent, shorter-chain compounds—were detected in the base traps at concentrations that account for up to 0.60 % and 0.16 % of the total fluorine initially present in treatments with and without methane, respectively (Fig. S11). Although this indicates thermal desorption is a potential PFAS mass removal pathway in the FB-GAP reactor, its contribution to the total mass loss is negligible. The concentration of the six parent PFAS was significant only in the first base trap, suggesting there is limited transport of fluorinated alkyl acids through the gas phase upon hydration. The concentrations were 3–5 times higher in the treatment with methane, which achieved temperatures 100–200 °C higher (Fig. S11c). The higher temperatures and the presence of water vapor may have facilitated the transport of PFAS through the off-gas. Carboxylic acids seem to be more easily desorbed/transported than the analogous sulfonic acids (Fig. S11), consistent with their comparatively lower boiling points [71]. Shorter chain PFAS were also detected (e.g., PFPeA, PFHxA, and PFHpA) albeit at lower concentrations, suggesting that the parent PFAS are transformed with and without methane. Note that a fraction of these PFAS may have resulted from thermal desorption of short-chain impurities (from the technical salts/acids used).

In the absence of methane, the pH of all four base traps was < 4 likely as a result of the formation of nitrogen (di)oxide in the air plasma discharge [82,83] with subsequent accumulation of nitric acid upon dissolution of these gases. Even with methane a pH drop was observed (from ~12.7 to ~8.5), but it was less pronounced than in the case with air only—CO_2 from methane combustion likely buffered the solution in the base traps through the formation of (bi)carbonate. A potential issue arising from the low pH in the run without methane is that part of the fluoride may be lost as HF (pK_a = 3.2). Therefore, the defluorination extents presented below may be conservative estimates.

Fluoride was only detected in the first base trap and accounted for up to 17 % and 2 % of the total fluorine in the methane and air only runs (Fig. 6). The amount of fluoride on the solids had the opposite trend (i.e., higher for the run without methane) and was consistent with the results presented in Fig. 5 despite the differences in absolute temperature developed in the reactor (Fig. 2 and S11). This resulted in a total defluorination—and, effectively, a fluorine mass balance—of 22 % and 16 % for the runs with and without methane, respectively (Fig. 6). The similarity in the defluorination extents may suggest that the fluorine that

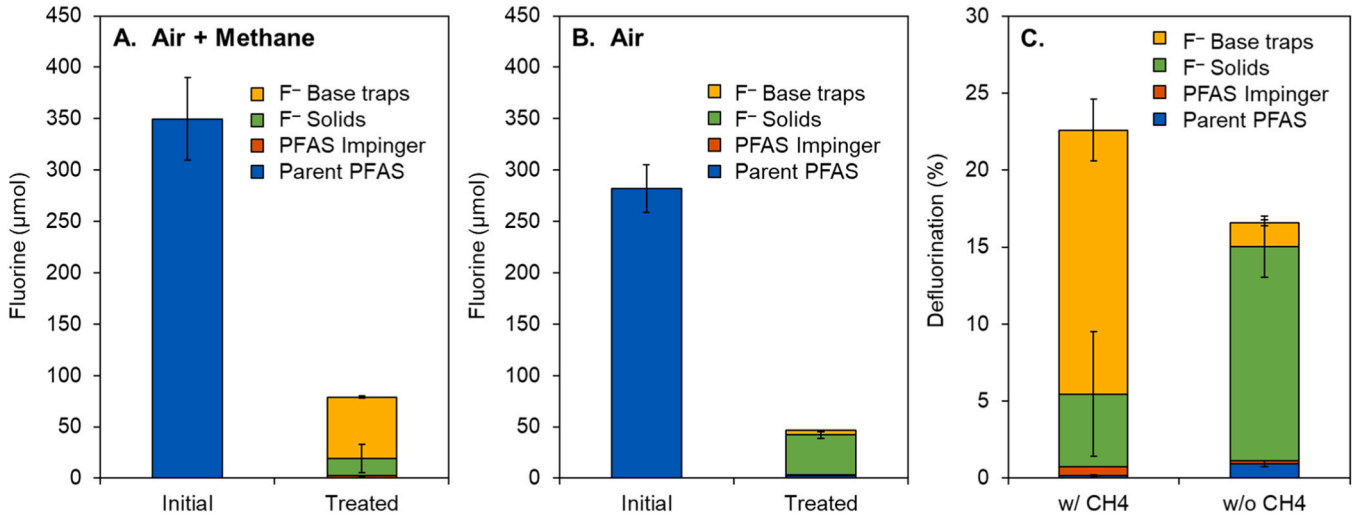


Fig. 6. Fluorine mass balance in the treatment with A. air (40 L/min) + CH_4 (2.5 L/min) at 250 W and B. air alone (40 L/min) at 700 W. Panel C. shows the defluorination extent—the parent PFAS on the solids and PFAS in the impingers are considered in the mass balance. Data represent the average ± one standard deviation of triplicate samples.

is "lost" from the solids in the presence of methane (as observed in Fig. 5), irrespective of its chemical form (e.g., SiF_4 or HF), is trapped in the impingers.

The gap in the fluorine mass balance could be a consequence of potential irreversible reactions between fluorine and SiO_2 (as described above) and/or the formation of gaseous products during the thermal degradation of PFAS (e.g., perfluorocarbons) that are not measurable by LC-QTOF-MS with ESI. While there is limited information on the PFAS degradation products during combustion reactions (i.e., thermal treatment under oxygen), Wang et al. showed that at the temperatures achieved in the FB-GAP (200–600 °C; Fig. S11c) unsaturated perfluorocarbons, perfluorinated acyl fluorides, and *1 H*-perfluoroalkanes are formed [76]. The preponderance of acyl fluorides is decreased when PFAS are pyrolyzed [76], but similar degradation products are observed: short and long chain (un)saturated perfluorocarbons [67,84], and in the presence of salts in the solid matrices, chlorinated and brominated perfluorocarbons [85]. Future work should evaluate the feasibility of recirculating the effluent gas and passing it through the gliding arc plasma discharge to further treat any (potentially formed) gaseous PIC. Our findings on treating PFAS-contaminated water reveal that direct exposure to the GAP discharge results in near-complete mineralization (defluorination) through a process that is not purely thermal [74]. Therefore, it is hypothesized that the highly reactive environment of the GAP discharges will mineralize any gaseous PFAS present in the recirculated gas.

4. Conclusions

The results from this study demonstrate that non-thermal plasma can be a viable treatment technology for dry PFAS-laden solids. While heat was found to be the main driver for the PFAS mass removals from contaminated solids, plasma-assisted combustion via the FB-GAP may be more advantageous than regular thermal processes because 1) it is a scalable process that reduces treatment costs through the combustion of lean-fuel mixtures (~26–50 % cost savings with the potential for further savings through optimization), and 2) any volatile organofluorine compounds *may* be further treated via recirculation of the off-gas through the highly reactive plasma discharges, potentially enabling complete PFAS mineralization. Without recirculation, the fluorine mass balance was ~20 %, with the remaining ~80 % likely present as volatile organofluorine compounds and/or products formed through irreversible reactions with SiO_2. Recirculation of the effluent gas through the GAP discharge may help to avoid expensive post-treatment/afterburner controls (treatment at > 1,000°C) and minimize the reliance on granular activated carbon (or other sorbents) to capture volatile products [79].

Environmental implications

The gliding arc plasmatron (GAP), a type of non-thermal plasma discharge, offers a scalable, energy-efficient solution for treating PFAS-contaminated solids. Unlike traditional thermal-based technologies, the potential for effluent gas recirculation within the GAP system may eliminate products of incomplete combustion (PIC) generated from the treated solids. Moreover, integrating plasma-assisted combustion into a fluidized bed configuration reduces treatment costs, making GAP a more sustainable and economically viable approach to PFAS remediation.

CRediT authorship contribution statement

Erica R. McKenzie: Writing – review & editing, Supervision, Resources, Project administration, Funding acquisition, Conceptualization. **Gregory Fridman:** Writing – review & editing, Conceptualization. **Alexander Fridman:** Conceptualization. **Christopher M. Sales:** Writing – review & editing, Supervision, Project administration, Funding acquisition, Conceptualization. **Alexander Rabinovich:** Writing – review & editing, Resources, Investigation. **Jimmy Murillo-Gelvez:** Writing – original draft, Visualization, Investigation, Formal analysis, Data curation, Conceptualization.

Declaration of Competing Interest

The authors declare the following financial interests/personal relationships which may be considered as potential competing interests: The authors have filed a provisional patent application for the FB-GAP reactor (#63/672,272) to Drexel University.

Acknowledgements

This research was supported by the Strategic Environmental Research and Development Program (SERDP) under project ER18–1570. The authors thank Alexandr Blackbay and Gary Nirenberg for their assistance in building and maintaining the FB-GAP reactors.

Supplementary data

The supplementary data including information on the reactors, QA/QCs, fluoride analyses, PFAS degradation profiles, first order kinetics, cost calculations, shorter chain PFAS, fluoride controls, and PFAS in the base traps (impingers) can be found in the online version of the article.

Appendix A. Supporting information

Supplementary data associated with this article can be found in the online version at doi:10.1016/j.jhazmat.2025.138678.

Data availability

Data will be made available on request.

References

[1] Schaider, L.A., Balan, S.A., Blum, A., Andrews, D.Q., Strynar, M.J., Dickinson, M.E., et al., 2017. Fluorinated compounds in U.S. fast food packaging. Environ Sci Technol Lett 4, 105–111. https://doi.org/10.1021/acs.estlett.6b00435.

[2] Jacob, P., Barzen-Hanson, K.A., Helbling, D.E., 2021. Target and nontarget analysis of per- and polyfluoralkyl substances in wastewater from electronics fabrication facilities. Environ Sci Technol 55, 2346–2356. https://doi.org/10.1021/acs.est.0c06690.

[3] Whitehead, H.D., Venier, M., Wu, Y., Eastman, E., Urbanik, S., Diamond, M.L., et al., 2021. Fluorinated compounds in North American cosmetics. Environ Sci Technol Lett 8, 538–544. https://doi.org/10.1021/acs.estlett.1c00240.

[4] van der Veen, I., Schellenberger, S., Hanning, A.-C., Stare, A., de Boer, J., Weiss, J. M., et al., 2022. Fate of per- and polyfluoroalkyl substances from durable water-repellent clothing during use. Environ Sci Technol 56, 5886–5897. https://doi.org/10.1021/acs.est.1c07876.

[5] Barzen-Hanson, K.A., Roberts, S.C., Choyke, S., Oetjen, K., McAlees, A., Riddell, N., et al., 2017. Discovery of 40 classes of per- and polyfluoroalkyl substances in historical aqueous film-forming foams (AFFFs) and AFFF-impacted groundwater. Environ Sci Technol 51, 2047–2057. https://doi.org/10.1021/acs.est.6b05843.

[6] Haukås, M., Berger, U., Hop, H., Gulliksen, B., Gabrielsen, G.W., 2007. Bioaccumulation of per- and polyfluorinated alkyl substances (PFAS) in selected species from the Barents Sea food web. Environ Pollut 148, 360–371. https://doi.org/10.1016/j.envpol.2006.09.021.

[7] Burkhard, L.P., 2021. Evaluation of published bioconcentration factor (BCF) and bioaccumulation factor (BAF) data for per- and polyfluoroalkyl substances across aquatic species. Environ Toxicol Chem 40, 1530–1543. https://doi.org/10.1002/etc.5010.

[8] Lewis, A.J., Yun, X., Spooner, D.E., Kurz, M.J., McKenzie, E.R., Sales, C.M., 2022. Exposure pathways and bioaccumulation of per- and polyfluoroalkyl substances in freshwater aquatic ecosystems: key considerations. Sci Total Environ 822, 153561. https://doi.org/10.1016/j.scitotenv.2022.153561.

[9] Khan, B., Burgess, R.M., Cantwell, M.G., 2023. Occurrence and bioaccumulation patterns of per- and polyfluoroalkyl substances (PFAS) in the marine environment. ACS EST Water 3, 1243–1259. https://doi.org/10.1021/acsestwater.2c00296.

[10] Pérez, F., Nadal, M., Navarro-Ortega, A., Fàbrega, F., Domingo, J.L., Barceló, D., et al., 2013. Accumulation of perfluoroalkyl substances in human tissues. Environ Int 59, 354–362. https://doi.org/10.1016/j.envint.2013.06.004.

[11] Bolan, N., Sarkar, B., Yan, Y., Li, Q., Wijesekara, H., Kannan, K., et al., 2021. Remediation of poly- and perfluoroalkyl substances (PFAS) contaminated soils – to mobilize or to immobilize or to degrade? J Hazard Mater 401, 123892. https://doi.org/10.1016/j.jhazmat.2020.123892.

[12] Brusseau, M.L., Anderson, R.H., Guo, B., 2020. PFAS concentrations in soils: background levels versus contaminated sites. Sci Total Environ 740, 140017. https://doi.org/10.1016/j.scitotenv.2020.140017.

[13] Xu, B., Liu, S., Zhou, J.L., Zheng, C., Weifeng, J., Chen, B., et al., 2021. PFAS and their substitutes in groundwater: occurrence, transformation and remediation. J Hazard Mater 412, 125159. https://doi.org/10.1016/j.jhazmat.2021.125159.

[14] Johnson, G.R., Brusseau, M.L., Carroll, K.C., Tick, G.R., Duncan, C.M., 2022. Global distributions, source-type dependencies, and concentration ranges of per- and polyfluoroalkyl substances in groundwater. Sci Total Environ 841, 156602. https://doi.org/10.1016/j.scitotenv.2022.156602.

[15] Pan, Y., Zhang, H., Cui, Q., Sheng, N., Yeung, L.W.Y., Sun, Y., et al., 2018. Worldwide distribution of novel perfluoroether carboxylic and sulfonic acids in surface water. Environ Sci Technol 52, 7621–7629. https://doi.org/10.1021/acs.est.8b00829.

[16] Podder, A., Sadmani, A.H.M.A., Reinhart, D., Chang, N.-B., Goel, R., 2021. Per and poly-fluoroalkyl substances (PFAS) as a contaminant of emerging concern in surface water: a transboundary review of their occurrences and toxicity effects. J Hazard Mater 419, 126361. https://doi.org/10.1016/j.jhazmat.2021.126361.

[17] Baabish, A., Sobhanei, S., Fiedler, H., 2021. Priority perfluoroalkyl substances in surface waters - a snapshot survey from 22 developing countries. Chemosphere 273, 129612. https://doi.org/10.1016/j.chemosphere.2021.129612.

[18] Li, R., Isowamwen, O.F., Ross, K.C., Holsen, T.M., Thagard, S.M., 2023. PFAS–CTAB complexation and its role on the removal of PFAS from a Lab-Prepared Water and a Reverse Osmosis Reject Water Using a Plasma Reactor. Environ Sci Technol 57, 12901–12910. https://doi.org/10.1021/acs.est.3c03679.

[19] Lewis, A.J., Joyce, T., Hadaya, M., Ebrahimi, F., Dragiev, I., Giardetti, N., et al., 2020. Rapid degradation of PFAS in aqueous solutions by reverse vortex flow gliding arc plasma. Environ Sci 6, 1044–1057. https://doi.org/10.1039/C9EW01050E.

[20] Papalexopoulou, K., Huang, X., Ronen, A., Aggelopoulos, C.A., 2024. Reactive species and mechanisms of perfluorooctanoic acid (PFOA) degradation in water by cold plasma: the role of HV waveform, reactor design, water matrix and plasma gas. Sep Purif Technol 342, 126955. https://doi.org/10.1016/j.seppur.2024.126955.

[21] Scheitlin, C.G., Dasu, K., Rosansky, S., Dejarme, L.E., Siriwardena, D., Thorn, J., et al., 2023. Application of supercritical water oxidation to effectively destroy per- and polyfluoroalkyl substances in aqueous matrices. ACS EST Water 3, 2053–2062. https://doi.org/10.1021/acsestwater.2c00548.

[22] Li, J., Austin, C., Moore, S., Pinkard, B.R., Novosselov, I.V., 2023. PFOS destruction in a continuous supercritical water oxidation reactor. Chem Eng J 451, 139063. https://doi.org/10.1016/j.cej.2022.139063.

[23] Wu, B., Hao, S., Choi, Y., Higgins, C.P., Deeb, R., Strathmann, T.J., 2019. Rapid destruction and defluorination of perfluorooctanesulfonate by alkaline hydrothermal reaction. Environ Sci Technol Lett 6, 630–636. https://doi.org/10.1021/acs.estlett.9b00506.

[24] Hao, S., Choi, Y.-J., Wu, B., Higgins, C.P., Deeb, R., Strathmann, T.J., 2021. Hydrothermal alkaline treatment for destruction of per- and polyfluoroalkyl substances in aqueous film-forming foam. Environ Sci Technol 55, 3283–3295. https://doi.org/10.1021/acs.est.0c06906.

[25] Liang, S., Pierce Jr, R. "David", Lin, H., Chiang, S.-Y. (Dora), Huang, Q. "Jack", 2018. Electrochemical oxidation of PFOA and PFOS in concentrated waste streams. Remediat J 28, 127–134. https://doi.org/10.1002/rem.21554.

[26] Smith, S.J., Lauria, M., Ahrens, L., McCleaf, P., Hollman, P., Bjälkefur Seroka, S., et al., 2023. Electrochemical oxidation for treatment of PFAS in contaminated water and fractionated foam—a pilot-scale study. ACS EST Water 3, 1201–1211. https://doi.org/10.1021/acsestwater.2c00660.

[27] Liu, Z., Bentel, M.J., Yu, Y., Ren, C., Gao, J., Pulikkal, V.F., et al., 2021. Near-quantitative defluorination of perfluorinated and fluorotelomer carboxylates and sulfonates with integrated oxidation and reduction. Environ Sci Technol 55, 7052–7062. https://doi.org/10.1021/acs.est.1c00353.

[28] Liu, Z., Chen, Z., Gao, J., Yu, Y., Men, Y., Gu, C., et al., 2022. Accelerated degradation of perfluorosulfonates and perfluorocarboxylates by UV/Sulfite + iodide: reaction mechanisms and system efficiencies. Environ Sci Technol 56, 3699–3709. https://doi.org/10.1021/acs.est.1c07608.

[29] Crownover, E., Oberle, D., Kluger, M., Heron, G., 2019. Perfluoroalkyl and polyfluoroalkyl substances thermal desorption evaluation. Remediat J 29, 77–81. https://doi.org/10.1002/rem.21623.

[30] Sörengård, M., Lindh, A.-S., Ahrens, L., 2020. Thermal desorption as a high removal remediation technique for soils contaminated with per- and polyfluoroalkyl substances (PFASs). PLoS One 15, e0234476. https://doi.org/10.1371/journal.pone.0234476.

[31] Duchesne, A.L., Brown, J.K., Patch, D.J., Major, D., Weber, K.P., Gerhard, J.I., 2020. Remediation of PFAS-contaminated soil and granular activated carbon by smoldering combustion. Environ Sci Technol 54, 12631–12640. https://doi.org/10.1021/acs.est.0c03058.

[32] Wang, J., Lin, Z., He, X., Song, M., Westerhoff, P., Doudrick, K., et al., 2022. Critical review of thermal decomposition of per- and polyfluoroalkyl substances: mechanisms and implications for thermal treatment processes. Environ Sci Technol 56, 5355–5370. https://doi.org/10.1021/acs.est.2c02251.

[33] DiStefano, R., Feliciano, T., Mimna, R.A., Redding, A.M., Matthis, J., 2022. Thermal destruction of PFAS during full-scale reactivation of PFAS-laden granular activated carbon. Remediat J 32, 231–238. https://doi.org/10.1002/rem.21735.

[34] Battye, N., Patch, D., Koch, I., Monteith, R., Roberts, D., O'Connor, N., et al., 2024. Mechanochemical degradation of per- and polyfluoroalkyl substances in soil using an industrial-scale horizontal ball mill with comparisons of key operational metrics. Sci Total Environ 928, 172274. https://doi.org/10.1016/j.scitotenv.2024.172274.

[35] Gobindlal, K., Zujovic, Z., Jaine, J., Weber, C.C., Sperry, J., 2023. Solvent-free, ambient temperature and pressure destruction of perfluorosulfonic acids under mechanochemical conditions: degradation intermediates and fluorine fate. Environ Sci Technol 57, 277–285. https://doi.org/10.1021/acs.est.2c06673.

[36] Quinnan, J., Morrell, C., Nagle, N., Maynard, K.G., 2022. Ex situ soil washing to remove PFAS adsorbed to soils from source zones. Remediat J 32, 151–166. https://doi.org/10.1002/rem.21727.

[37] Uwayezu, J.N., Ren, Z., Sonnenschein, S., Leiviskä, T., Lejon, T., van Hees, P., et al., 2024. Combination of separation and degradation methods after PFAS soil washing. Sci Total Environ 907, 168137. https://doi.org/10.1016/j.scitotenv.2023.168137.

[38] Pang, H., Dorian, B., Gao, L., Xie, Z., Cran, M., Muthukumaran, S., et al., 2022. Remediation of poly-and perfluoroalkyl substances (PFAS) contaminated soil using gas fractionation enhanced technology. Sci Total Environ 827, 154310. https://doi.org/10.1016/j.scitotenv.2022.154310.

[39] Shahsavari, E., Rouch, D., Khudur, L.S., Thomas, D., Aburto-Medina, A., Ball, A.S., 2021. Challenges and current status of the biological treatment of PFAS-contaminated soils. Front Bioeng Biotechnol 8. ⟨https://www.frontiersin.org/journals/bioengineering-and-biotechnology/articles/10.3389/fbioe.2020.602040⟩.

[40] Wilton, G.M., Gerhard, J.I., Major, D.W., 2022. Carbon injection to support in-situ smoldering remediation. Remediat J 33, 39–51. https://doi.org/10.1002/rem.21737.

[41] Longendyke, G.K., Katel, S., Wang, Y., 2022. PFAS fate and destruction mechanisms during thermal treatment: a comprehensive review. Environ Sci Process Impacts 24, 196–208. https://doi.org/10.1039/D1EM00465D.

[42] Mattila, J.M., Krug, J.D., Roberson, W.R., Burnette, R.P., McDonald, S., Virtaranta, L., et al., 2024. Characterizing volatile emissions and combustion byproducts from aqueous film-forming foams using online chemical ionization mass spectrometry. Environ Sci Technol 58, 3942–3952. https://doi.org/10.1021/acs.est.3c09255.

[43] Weber, N.H., Redfern, H., Grimison, C.C., Lucas, J.A., Mackie, J.C., Stockenhuber, M., et al., 2024. Formation of products of incomplete destruction (PID) from the thermal oxidative decomposition of perfluorooctanoic acid (PFOA): measurement, modeling, and reaction pathways. J Phys Chem A 128, 5362–5373. https://doi.org/10.1021/acs.jpca.4c01909.

[44] Weitz, K., Kantner, D., Kessler, A., Key, H., Larson, J., Bodnar, W., et al., 2024. Review of per- and poly-fluoroalkyl treatment in combustion-based thermal waste systems in the United States. Sci Total Environ 932, 172658. https://doi.org/10.1016/j.scitotenv.2024.172658.

[45] Singh, R.K., Fernando, S., Baygi, S.F., Multari, N., Thagard, S.M., Holsen, T.M., 2019. Breakdown products from perfluorinated alkyl substances (PFAS) degradation in a plasma-based water treatment process. Environ Sci Technol 53, 2731–2738. https://doi.org/10.1021/acs.est.8b07031.

[46] Lewis, A.J., Joyce, T., Hadaya, M., Ebrahimi, F., Dragiev, I., Giardetti, N., et al., 2020. Rapid degradation of PFAS in aqueous solutions by reverse vortex flow gliding arc plasma. Environ Sci 6, 1044–1057. https://doi.org/10.1039/C9EW01050E.

[47] Alam, D., Lee, S., Hong, J., Fletcher, D.F., McClure, D., Cook, D., et al., 2023. Experimental investigations of Per- and Poly-fluoroalkyl substances (PFAS) degradation by non-thermal plasma in aqueous solutions. J Environ Chem Eng 11, 111588. https://doi.org/10.1016/j.jece.2023.111588.

[48] Bruggeman, P.J., Iza, F., Brandenburg, R., 2017. Foundations of atmospheric pressure non-equilibrium plasmas. Plasma Sources Sci Technol 26, 123002. https://doi.org/10.1088/1361-6595/aa97af.

[49] Bruggeman, P., Leys, C., 2009. Non-thermal plasmas in and in contact with liquids. J Phys D Appl Phys 42, 053001. https://doi.org/10.1088/0022-3727/42/5/053001.

[50] Zhan, J., Zhang, A., Héroux, P., Guo, Y., Sun, Z., Li, Z., et al., 2020. Remediation of perfluorooctanoic acid (PFOA) polluted soil using pulsed corona discharge plasma. J Hazard Mater 387, 121688. https://doi.org/10.1016/j.jhazmat.2019.121688.

[51] Kalghatgi, S., Kelly, C.M., Cerchar, E., Torabi, B., Alekseev, O., Fridman, A., et al., 2011. Effects of non-thermal plasma on mammalian cells. PLoS One 6, e16270. https://doi.org/10.1371/journal.pone.0016270.

[52] Nickerson, A., Maizel, A.C., Kulkarni, P.R., Adamson, D.T., Kornuc, J.J., Higgins, C. P., 2020. Enhanced extraction of AFFF-associated PFASs from source zone soils. Environ Sci Technol 54, 4952–4962. https://doi.org/10.1021/acs.est.0c00792.

[53] Yun, X., Lewis, A.J., Stevens-King, G., Sales, C.M., Spooner, D.E., Kurz, M.J., et al., 2023. Bioaccumulation of per- and polyfluoroalkyl substances by freshwater benthic macroinvertebrates: impact of species and sediment organic carbon content. Sci Total Environ 866, 161208. https://doi.org/10.1016/j.scitotenv.2022.161208.

[54] Buykx, S.E.J., van den Hoop, M.A.G.T., de Joode, P., 2004. Simultaneous extraction of bromide, chloride, fluoride and sulfate from soils, waste- and building materials. J Environ Monit 6, 552–558. https://doi.org/10.1039/B400378K.

[55] Chatterjee, A., Pan, N., Maji, T.K., Pasha, S.S., Singh, S., Ahmed, S.A., et al., 2021. Highly sensitive optical sensor for selective detection of fluoride level in drinking water: methodology to fabrication of prototype device. ACS Sustain Chem Eng 9, 7160–7170. https://doi.org/10.1021/acssuschemeng.1c02101.

[56] Bolton, J.R., Bircher, K.G., Tumas, W., Tolman, C.A., 1996. Figures-of-merit for the technical development and application of advanced oxidation processes. J. Adv. Oxid. Technol. 1, 13–17. https://doi.org/10.1515/jaots-1996-0104.

[57] Stratton, G.R., Dai, F., Bellona, C.L., Holsen, T.M., Dickenson, E.R.V., Mededovic Thagard, S., 2017. Plasma-based water treatment: efficient transformation of perfluoroalkyl substances in prepared solutions and contaminated groundwater. Environ Sci Technol 51, 1643–1648. https://doi.org/10.1021/acs.est.6b04215.

[58] Isowamwen, O., Li, R., Holsen, T., Thagard, S.M., 2023. Plasma-assisted degradation of a short-chain perfluoroalkyl substance (PFAS): perfluorobutane sulfonate (PFBS). J Hazard Mater 456, 131691. https://doi.org/10.1016/j.jhazmat.2023.131691.

[59] Surace, M.J., Murillo-Gelvez, J., Shaji, M.A., Fridman, A.A., Rabinovich, A., McKenzie, E.R., et al., 2023. Plasma-assisted abatement of per- and polyfluoroalkyl substances (PFAS): thermodynamic analysis and validation in gliding arc discharge. Plasma 6, 419–434. https://doi.org/10.3390/plasma6030029.

[60] Abdel-Salam, M., 2018. High-Voltage Engineering: Theory and Practice, Second Edition, Revised and Expanded. CRC Press. ⟨https://books.google.com/books?id=vUtZDwAAQBAJ⟩.

[61] Takamatsu, T., Uehara, K., Sasaki, Y., Miyahara, H., Matsumura, Y., Iwasawa, A., et al., 2014. Investigation of reactive species using various gas plasmas. RSC Adv 4, 39901–39905. https://doi.org/10.1039/C4RA05936K.

[62] Mohades, S., Lietz, A.M., Kushner, M.J., 2020. Generation of reactive species in water film dielectric barrier discharges sustained in argon, helium, air, oxygen and nitrogen. J Phys D Appl Phys 53, 435206. https://doi.org/10.1088/1361-6463/aba21a.

[63] Xiao, F., Sasi, P.C., Yao, B., Kubátová, A., Golovko, S.A., Golovko, M.Y., et al., 2020. Thermal stability and decomposition of perfluoroalkyl substances on spent granular activated carbon. Environ Sci Technol Lett 7, 343–350. https://doi.org/10.1021/acs.estlett.0c00114.

[64] Al Amin, M., Luo, Y., Nolan, A., Mallavarapu, M., Naidu, R., Fang, C., 2023. Thermal kinetics of PFAS and precursors in soil: experiment and surface simulation in temperature-time plane. Chemosphere 318, 138012. https://doi.org/10.1016/j.chemosphere.2023.138012.

[65] Blotevogel, J., Giraud, R.J., Rappé, A.K., 2023. Incinerability of PFOA and HFPO-DA: mechanisms, kinetics, and thermal stability ranking. Chem Eng J 457, 141235. https://doi.org/10.1016/j.cej.2022.141235.

[66] Sasi, P.C., Alinezhad, A., Yao, B., Kubátová, A., Golovko, S.A., Golovko, M.Y., et al., 2021. Effect of granular activated carbon and other porous materials on thermal decomposition of per- and polyfluoroalkyl substances: mechanisms and implications for water purification. Water Res 200, 117271. https://doi.org/10.1016/j.watres.2021.117271.

[67] Alinezhad, A., Challa Sasi, P., Zhang, P., Yao, B., Kubátová, A., Golovko, S.A., et al., 2022. An investigation of thermal air degradation and pyrolysis of per- and polyfluoroalkyl substances and aqueous film-forming foams in soil. ACS EST Eng 2, 198–209. https://doi.org/10.1021/acsestengg.1c00335.

[68] Ju, Y., Sun, W., 2015. Plasma assisted combustion: dynamics and chemistry. Prog Energy Combust Sci 48, 21–83. https://doi.org/10.1016/j.pecs.2014.12.002.

[69] Manz, K.E., Kulaots, I., Greenley, C.A., Landry, P.J., Lakshmi, K.V., Woodcock, M. J., et al., 2023. Low-temperature persulfate activation by powdered activated carbon for simultaneous destruction of perfluorinated carboxylic acids and 1,4-dioxane. J Hazard Mater 442, 129966. https://doi.org/10.1016/j.jhazmat.2022.129966.

[70] Briels, N., Ciesielski, T.M., Herzke, D., Jaspers, V.L.B., 2018. Developmental toxicity of perfluorooctanesulfonate (PFOS) and its chlorinated polyfluoroalkyl ether sulfonate alternative F-53B in the domestic chicken. Environ Sci Technol 52, 12859–12867. https://doi.org/10.1021/acs.est.8b04749.

[71] Xiao, F., Challa Sasi, P., Alinezhad, A., Sun, R., Abdulmalik Ali, M., 2023. Thermal phase transition and rapid degradation of forever chemicals (PFAS) in spent media using induction heating. ACS EST Eng 3, 1370–1380. https://doi.org/10.1021/acsestengg.3c00114.

[72] Zhu, D., Sun, Z., Zhang, H., Zhang, A., Zhang, Y., Miruka, A.C., et al., 2022. Reactive nitrogen species generated by gas–liquid dielectric barrier discharge for efficient degradation of perfluorooctanoic acid from water. Environ Sci Technol 56, 349–360. https://doi.org/10.1021/acs.est.1c06342.

[73] Aggelopoulos, C.A., 2022. Recent advances of cold plasma technology for water and soil remediation: a critical review. Chem Eng J 428, 131657. https://doi.org/10.1016/j.cej.2021.131657.

[74] Shaji, M.A., Surace, M.J., Rabinovich, A., Sales, C.M., Fridman, G., McKenzie, E.R., et al., 2024. Investigating the effects of gliding arc plasma discharge's thermal characteristic and reactive chemistry on aqueous PFOS mineralization. Plasma 7, 705–720. https://doi.org/10.3390/plasma7030036.

[75] El-Attar, H.A., Jackson, M.L., Volk, V.V., 1972. Fluorine loss from silicates on ignition. Am Mineral 57, 246–252.

[76] Wang, J., Song, M., Abusallout, I., Hanigan, D., 2023. Thermal decomposition of two gaseous perfluorocarboxylic acids: products and mechanisms. Environ Sci Technol 57, 6179–6187. https://doi.org/10.1021/acs.est.2c08210.

[77] Sennikov, P.G., Ikrin, M.A., Ignatov, S.K., Bagatur'yants, A.A., Klimov, E.Yu, 1999. IR spectroscopic andab initio quantum-chemical study of the products of hydrolysis of silicon tetrafluoride at low water concentrations. Russ Chem Bull 48, 93–97. https://doi.org/10.1007/BF02494407.

[78] Finney, W.F., Wilson, E., Callender, A., Morris, M.D., Beck, L.W., 2006. Reexamination of hexafluorosilicate hydrolysis by ^{19}F NMR and pH measurement. Environ Sci Technol 40, 2572–2577. https://doi.org/10.1021/es052295s.

[79] Wang, J., Lin, Z., He, X., Song, M., Westerhoff, P., Doudrick, K., et al., 2022. Critical review of thermal decomposition of per- and polyfluoroalkyl substances: mechanisms and implications for thermal treatment processes. Environ Sci Technol 56, 5355–5370. https://doi.org/10.1021/acs.est.2c02251.

[80] Khan, M.Y., So, S., da Silva, G., 2020. Decomposition kinetics of perfluorinated sulfonic acids. Chemosphere 238, 124615. https://doi.org/10.1016/j.chemosphere.2019.124615.

[81] Khan, M.Y., Song, J., Narimani, M., da Silva, G., 2022. Thermal decomposition mechanism and kinetics of perfluorooctanoic acid (PFOA) and other perfluorinated carboxylic acids: a theoretical study. Environ Sci Process Impacts 24, 2475–2487. https://doi.org/10.1039/D2EM00259K.

[82] Bae, J.H., Lee, H., Huh, S.-C., Park, S., 2024. Nitric and nitrous acid formation in plasma-treated water: decisive role of nitrogen oxides (NOx=1–3). Chemosphere, 143105. https://doi.org/10.1016/j.chemosphere.2024.143105.

[83] Rouwenhorst, K.H.R., Jardali, F., Bogaerts, A., Lefferts, L., 2021. From the Birkeland–Eyde process towards energy-efficient plasma-based NOX synthesis: a techno-economic analysis. Energy Environ Sci 14, 2520–2534. https://doi.org/10.1039/D0EE03763J.

[84] Hughey, K.D., Gallagher, N.B., Zhao, Y., Thakur, N., Bradley, A.M., Koster van Groos, P.G., et al., 2024. PFAS remediation: evaluating the infrared spectra of complex gaseous mixtures to determine the efficacy of thermal decomposition of PFAS. Chemosphere 362, 142631. https://doi.org/10.1016/j.chemosphere.2024.142631.

[85] Zhao, Y., Koster van Groos, P.G., Thakur, N., Fuller, M.E., Soto, A., Hatzinger, P.B., 2024. Formation of volatile chlorinated and brominated products during low temperature thermal decomposition of the representative PFAS perfluorohexane sulfonate (PFHxS) in the presence of NaCl and NaBr. Environ Pollut 348, 123782. https://doi.org/10.1016/j.envpol.2024.123782.